PERGAMON

Journal of Structural Geology 22 (2000) 1341–1358

JOURNAL OF STRUCTURAL GEOLOGY

www.elsevier.nl/locate/jstrugeo

Rock deformation tests to large shear strains in torsion

M.S. Paterson[a], D.L. Olgaard[b,*]

[a]*Research School of Earth Sciences, Australian National University, Canberra, Australia*
[b]*Geologisches Institut, Eidgenössische Technisches Hochschule (ETH), Zürich, Switzerland*

Received 16 August 1999; accepted 10 April 2000

Abstract

Experiments performed to high strains in simple shear are necessary to resolve many important problems in rock deformation, including the simulation of non-coaxial deformation, the exploration of the influence of strain on rheology, and the development of mineral segregation, dynamic recrystallisation, and other aspects of microstructure. Using a new torsion system we are able to simulate both the high strains and the simple shear style commonly observed in naturally deformed rocks, and to make accurate measurements of shear stress, strain and strain rate at high temperatures and pressures. The torsion system, which is described briefly, is based on a standard gas-medium high-pressure high-temperature triaxial deformation machine to which has been added an additional module allowing rotary shear of a cylindrical specimen.

In this paper, we discuss procedures for carrying out torsion tests and we analyse the mechanics of torsional deformation. We show how to extract information about the rheological parameters from the torque–twist data, and how to deal with the problems posed by the variation of strain within a cylindrical specimen. Procedures for microstructural studies are also set out. Finally, some results on calcite rocks are given to illustrate the application of torsion tests.

1. Introduction

Experimental rock deformation studies of potential geological application have so far concentrated mainly on coaxial axisymmetric deformation, as typified by the so-called 'triaxial test'. However, many geological deformation histories are non-coaxial and relatively few experimental studies have been carried out which are of relevance to them. Therefore, in order to facilitate such experimentation at high temperature and high confining pressure, a torsion testing system has been developed for use in a gas-medium testing machine. The present paper discusses the application of this testing system in the context of general aspects of torsion testing.

Geological deformation is commonly non-coaxial, or rotational, in the sense that the principal axes of strain lie parallel to different lines of particles in successive strain increments, that is, the axes rotate. Simple shear is a non-coaxial deformation. Geological examples of non-coaxial deformations are seen in the limbs of folds and, most notably, in shear zones (Ramsay, 1980). Shear zones occur on many scales, from the tectonic scale, as represented in the Glarus Thrust in Switzerland (Schmid, 1975), to the local scale of millimetres, as illustrated in figure 5.38 of Hobbs et al. (1976). Shear zones represent a localisation of deformation, generally resulting from rheological instability. The magnitude of the strain can be very high and the large strains can lead to characteristic textures and fabrics in the rocks, as in mylonites, the symmetry of which tends to reflect the symmetry of the deformation. It is often difficult to determine the strain exactly but shear strains γ of at least 10–20 have been reported (Ramsay and Graham, 1970). The corresponding maximum natural extensional strain ε can be obtained from

* Corresponding author. Fax: +1-713-431-6115. Now at: Exxon Mobil Upstream Research Company, PO Box 2189, Houston, Texas, USA.

E-mail address: dlolgaa@upstream.xomcorp.com (D.L. Olgaard).

0191-8141/00/$ - see front matter
PII: S0191-8141(00)00042-0

$$\varepsilon = \ln \sqrt{\frac{1}{2}\left(2 + \gamma^2 + \gamma\sqrt{4 + \gamma^2}\right)} \quad (1)$$

$$\text{or } \varepsilon = \ln \gamma \text{ for large } \gamma \quad (2)$$

(Ramsay, 1980; Ramsay and Huber, 1983).

The features associated with large geological shear strains can be conveniently explored experimentally in torsion tests on cylindrical specimens (Fig. 1). The aims of such tests therefore include:

1. To carry out non-coaxial deformation.
2. To explore rheological and microstructural development over a much larger strain range.

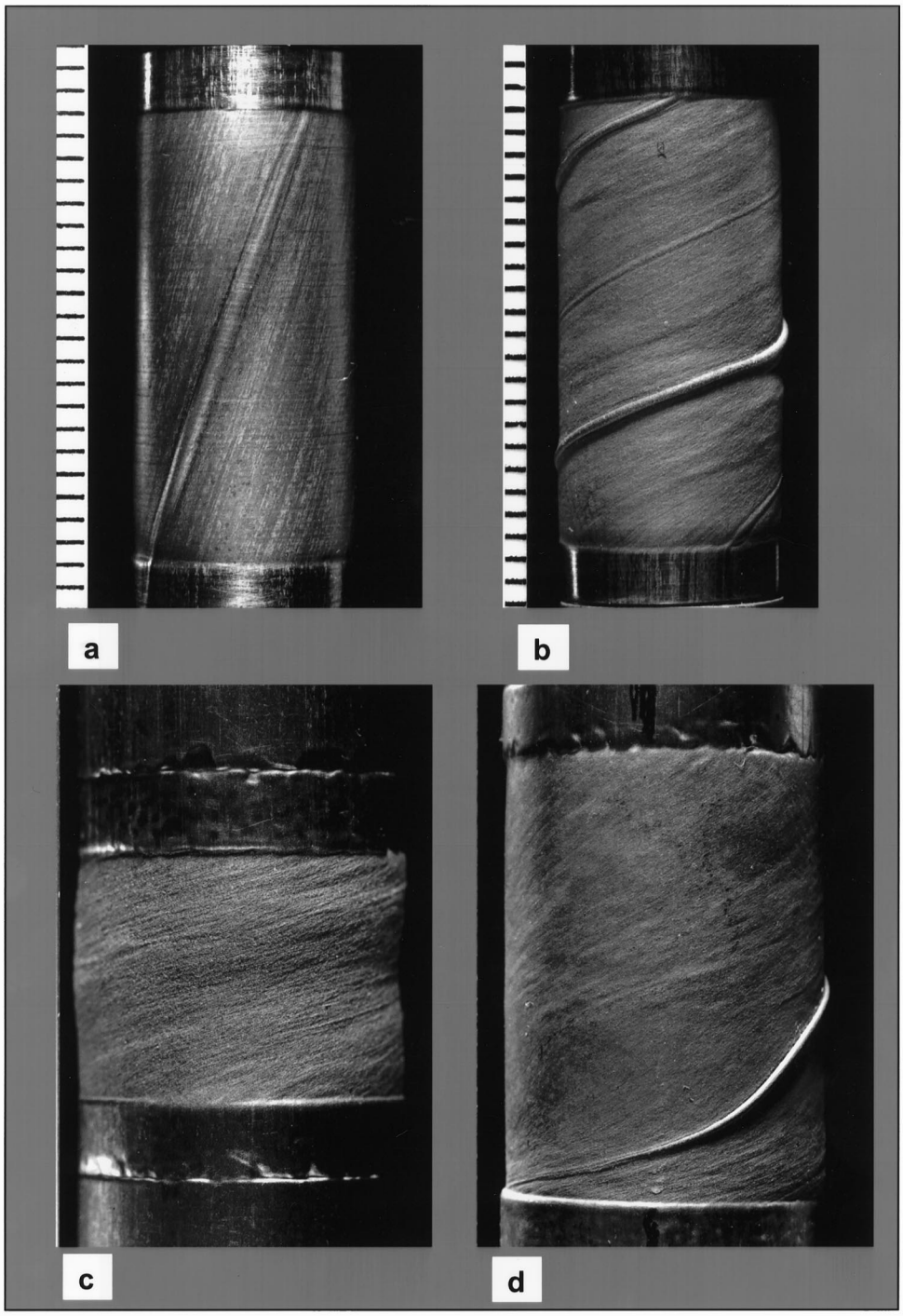

Fig. 1. Torsion specimens of Carrara marble. These specimens have been deformed between alumina pistons, the whole assembly being enclosed in a thin iron jacket; wrinkles in the jacket, originally parallel to the axis, serve as markers for the deformation. (a) 10 mm diameter, $\gamma = 0.6$; (b) 10-mm diameter, $\gamma = 2.1$; (c) 15 mm diameter, $\gamma = 5$; (d) 15 mm diameter, γ varying from 1 to >10 (Urs Gerber).

3. To explore the development of localisation of deformation in shear.
4. To study the fabric and texture produced by large non-coaxial strains.

By applying axial loading in addition to torsional loading, using hollow cylinders if necessary, general rheological behaviour can also be explored since all three principal stresses can then be varied independently.

The achievement of large strains is in itself of considerable interest in connection with both rheological and microstructural development. Strains in triaxial experiments in compression are usually limited to 0.2–0.3 for rheological purposes because of complications associated with inhomogeneous behaviour such as barrelling and buckling, although with the lateral constraints of solid medium apparatus strains several times greater have been achieved for microstructural studies (Tullis and Yund, 1977; Dell'Angelo and Tullis, 1996). Large strains can be achieved in extension and Rutter (1998) has shown how to analyse the measurements on necked specimens to yield data on coaxial mechanical behaviour to natural strains of around 2. The importance of exploring behaviour to such strains is that microstructural development such as recrystallisation is commonly still incomplete after strains of 0.2–0.3 and it is questionable whether a mechanical steady state has yet been established. Preliminary results mentioned later indicate that in the case of marble and anhydrite a steady state is not reached until at least a shear strain of 2. Shear strains of this order can be achieved in diagonal saw-cut tests (for example, Dell'Angelo et al., 1987; Schmid et al., 1987; Zhang and Karato, 1995) but the constraints brought into play by the lateral offsets can be expected to complicate the derivation of accurate strength data at the higher strains.

The torsion test has many advantages for testing to high strains, as follows:

1. There is no limit to the amount of twist that can be applied to the specimen.
2. In the absence of material instability the deformation is homogeneous to a high degree (Fig. 1a–c). Thus there is no 'end effect' similar to the conical zone adjacent to the loading anvils in axial tests because all displacements are parallel to the ends. The geometry remains essentially unchanged throughout the deformation to large strains, greatly facilitating the establishment of whether a steady state is developed or not.
3. Localisation of strain due to material instability is readily studied in specimens of moderate length because of the absence of any lateral constraints on the specimen (Fig. 1d).
4. The local deformation in the specimen is always a simple shear although on the scale of the specimen the shear direction curves around the cylindrical axis (Fig. 1b).

Torsion tests on cylindrical specimens have often been used in materials science (for example, Swift, 1947; Hardwick and Tegart, 1961; Keane et al., 1966; Lindholm et al., 1981; Canova et al., 1982; Montheillet et al., 1984; Tóth et al., 1992; Blankenship et al., 1995), but only rarely in experimental rock deformation. An early application to rocks was that of Boeker (1915) and the most comprehensive studies were those of Handin et al. (1960, 1967). Durand and Comes (1974), Durand (1975) and Bouchez and Duval (1982) have used torsion tests in studies on ice. In addition, the rotating anvil method of Bridgman (1935, 1936) has been applied by Carter et al. (1964) and by Riecker and Seifert (1964a,b), Riecker (1965) and Riecker and Rooney (1966, 1967, 1969) to shear deformation of various geological materials at high temperatures, but this procedure only produces a thin layer of deformed material and does not yield accurate rheological data. Somewhat similar experiments have been carried out on analogue materials by Jessell and Lister (1991) and Bons and Urai (1996). Friction experiments in torsion can also be used to study large shear strains in gouge (for example, Tullis and Weeks, 1986; Yund et al., 1990; Tullis, 1994).

2. Mechanics of the torsion test

2.1. Basic analysis

The mechanics of the torsion test are well known (e.g. Metals Handbook, 1985). Here we consider the torsion of an isotropic homogenous cylindrical specimen of diameter d and length l, to which is applied a torque M, and we designate the amount of twist or

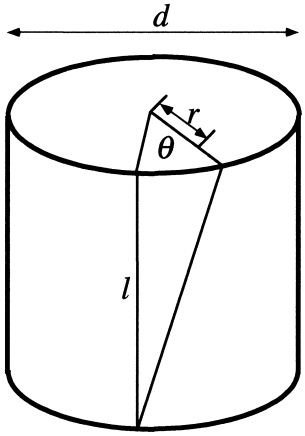

Fig. 2. Schematic diagram of cylindrical specimen.

angular displacement by θ. The strain in the specimen is inhomogeneous, being zero at the central axis and a maximum at the cylindrical surface. However, because of the constraints of the geometry, planes of material normal to the axis will remain planar, and radial lines of material normal to the axis will remain linear. Any element along a radius of the cylinder undergoes a simple shear in a plane normal to the radius, the displacements being in the direction normal to the cylinder axis (Fig. 2). The shear strain γ_r at any radius r is then given by $\gamma_r = r\theta/l$ and so the strain rate at any given radius r is given by $\dot{\gamma}_r = r\dot{\theta}/l$. Therefore, the strain and the strain rate increase linearly with radius within the specimen.

The maximum shear strain γ, at the surface of the cylinder, is given by

$$\gamma = \frac{d\theta}{2l} \tag{3}$$

and the corresponding maximum strain rate $\dot{\gamma}$ is given by

$$\dot{\gamma} = \frac{d\dot{\theta}}{2l} = \frac{\pi d\omega}{l} \tag{4}$$

where $\dot{\theta}$ and ω are the twist rate in radians per second and in revolutions per second, respectively.

The stress state in the specimen will depend on the stress–strain characteristics of the material but will be of cylindrical symmetry for isotropic and homogeneous material. For each annular ring of width dr at radius r, in which the shear stress is τ_r, the torque is $\tau_r 2\pi r^2\,\mathrm{d}r$ and therefore the total torque M is given by

$$M = 2\pi \int \tau_r r^2\,\mathrm{d}r. \tag{5}$$

The evaluation of this integral depends on the specific stress–strain relationship, as follows:

For the elastic case, if we assume that $\tau_r = G\gamma_r$ where G is the shear modulus, we obtain for a solid cylinder

$$M = \frac{\pi G\theta d^4}{32l} = \frac{\pi d^3\tau}{16} \tag{6}$$

since the maximum shear stress at the surface, τ, is equal to $G\gamma = G\theta d/2l$. For a hollow cylinder of outside diameter d_o and inside diameter d_i we obtain

$$M = \frac{\pi G\theta\left(d_o^4 - d_i^4\right)}{32l} = \frac{\pi\left(d_o^4 - d_i^4\right)\tau}{16d_o}. \tag{7}$$

For the rigid-plastic case, in the case of a perfectly plastic material with yield stress τ_y, we have $\tau_r = \tau_y$ for all r, and we obtain for a solid cylinder

$$M = \frac{\pi d^3\tau_y}{12} \tag{8}$$

and for a hollow cylinder

$$M = \frac{\pi\left(d_o^3 - d_i^3\right)\tau_y}{12} \tag{9}$$

Power-law creep case:

Now we assume that $\dot{\gamma}_r = A\tau_r^n\,\mathrm{e}^{\frac{-Q}{RT}}$, where A, n and Q are constants, T is the temperature, and R is the gas constant, so that $\tau_r = (2r/d)^{1/n}\tau$, from which we obtain for a solid cylinder

$$M = \frac{\pi d^3\tau}{4\left(3 + \frac{1}{n}\right)} \tag{10}$$

and for a hollow cylinder

$$M = \frac{\pi\tau}{4\left(3 + \frac{1}{n}\right)} \frac{d_o^{3+\frac{1}{n}} - d_i^{3+\frac{1}{n}}}{d_o^{\frac{1}{n}}} \tag{11}$$

It is noted that, for $n = 1$ and $n = \infty$, the expressions Eqs. (10) and (11) correspond, respectively, to Eqs. (6) and (7), and to Eqs. (8) and (9). Also, since M is linearly related to τ, the slope of the log–log plot of $\dot{\gamma}$ or $\dot{\theta}$ vs. M for constant temperature will give the value of n in a way analogous to the procedure in axial deformation tests, that is,

$$n = \frac{\mathrm{d}\ln\dot{\gamma}}{\mathrm{d}\ln M} = \frac{\mathrm{d}\ln\dot{\theta}}{\mathrm{d}\ln M}. \tag{12}$$

Similarly Q can be determined for constant strain rate using the expression

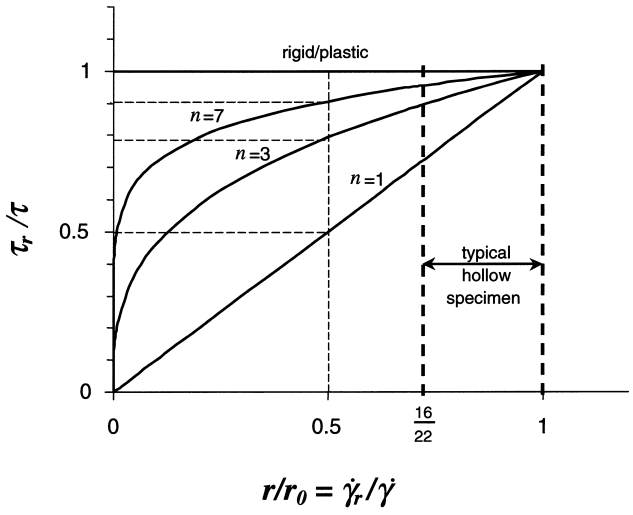

Fig. 3. Variation in shear stress τ_r with radius r for power law creep in dependence on stress exponent n; τ is the stress at the outer radius r_o.

$$Q = nR\frac{\mathrm{d}\ln M}{\mathrm{d}(1/T)}. \tag{13}$$

Having determined n and Q, A can be determined for given M and $\dot{\theta}$ from

$$A = \left(\frac{\pi d^{3+\frac{1}{n}}}{4M\left(3+\frac{1}{n}\right)}\right)^n \frac{\dot{\theta}\,\mathrm{e}^{\frac{Q}{RT}}}{2l}. \tag{14}$$

It must be borne in mind that the above analysis assumes homogeneous rheological properties throughout the specimen.

The nature of the radial variation in stress within the specimen as a function of its rheology is shown in Fig. 3.

2.2. Effect of non-uniform diameter or temperature — power-law creep case

There may be situations, such as those involving very strong samples or studies of localisation, in which it is desired to vary the diameter of the specimen in order to increase the degree of gripping at the ends or to concentrate the deformation in a controlled way, or to vary the temperature along the specimen. In these cases, the strain rate will also be non-uniform along the length. However, for equilibrium, the torque must be the same at all positions. This condition permits the calculation of distribution of maximum strain rate and stress along the length of the specimen.

If we consider the deformation of an elementary slice of thickness $\mathrm{d}x$ and diameter d_x at distance x from the reference end of a specimen of total length l, then, from Eq. (4), the contribution $\dot{\theta}_x$ from this element to the total twist rate $\dot{\theta}$ is given by

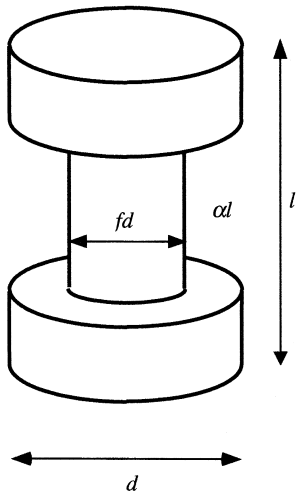

Fig. 4. Cylindrical specimen of non-uniform diameter.

$$\dot{\theta}_x = \frac{2\dot{\gamma}_x \mathrm{d}x}{d_x} \tag{15}$$

where $\dot{\gamma}_x$ is the maximum shear strain rate in the elementary slice. In the case of power-law creep, using Eq. (10), we can write

$$\dot{\gamma}_x = A\,\mathrm{e}^{\frac{-Q}{RT_x}}\tau_x^n = A\,\mathrm{e}^{\frac{-Q}{RT_x}}\left(\frac{4\left(3+\frac{1}{n}\right)}{\pi d_x^3}M\right)^n. \tag{16}$$

Then, for a given temperature profile T_x,

$$\dot{\theta} = \int_0^l \dot{\theta}_x \mathrm{d}x = 2A\left(\frac{4}{\pi}\left(3+\frac{1}{n}\right)\right)^n M^n \int_0^l \frac{\mathrm{e}^{\frac{-Q}{RT_x}}}{d_x^{3n+1}}\,\mathrm{d}x. \tag{17}$$

In the case of uniform temperature T where the diameter d is reduced to fd over a fraction α of the length l (Fig. 4), the integral term in Eq. (17) becomes

$$\int_0^l \frac{\mathrm{e}^{\frac{-Q}{RT_x}}}{d_x^{3n+1}}\,\mathrm{d}x = \frac{l\,\mathrm{e}^{\frac{-Q}{RT}}}{d^{3n+1}}\left((1-\alpha)+\frac{\alpha}{f^{\,3n+1}}\right) \tag{18}$$

and so the fractional contribution $\Delta\dot{\theta}_\alpha$ from the reduced section to the total twist rate $\dot{\theta}$ will be

$$\frac{\Delta\dot{\theta}_\alpha}{\dot{\theta}} = \frac{\frac{\alpha}{f^{\,3n+1}}}{1-\alpha+\frac{\alpha}{f^{\,3n+1}}} = \frac{\alpha}{\alpha+(1+\alpha)f^{\,3n+1}}. \tag{19}$$

Table 1 shows the degree of concentration of the deformation in the section of reduced diameter for various values of the parameters α, f and n. For example, if the specimen of material with $n = 3$ is reduced to 90% of its original diameter over 10% of its length, the reduced section will contribute 24% of the total twist; consequently, the strain in the reduced section will be 2.16γ and the strain in the remainder will be 0.84γ where γ is the apparent strain calculated from the total twist.

Similar considerations show that if there is a temperature gradient along the specimen, the total twist rate will be given by

Table 1
Examples of concentrated deformation, from Eq. (19)

α	f	N	$\frac{\alpha}{\alpha+(1-\alpha)f^{\,3n+1}}$
0.1	0.9	1	0.14
0.1	0.9	3	0.24
0.1	0.9	10	0.74
0.5	0.7	1	0.81
0.5	0.7	3	0.97
0.5	0.7	10	1.00

$$\dot{\theta} = \int_0^l \dot{\theta}_x \, dx = 2A\left(\frac{4}{\pi}\left(3 + \frac{1}{n}\right)\right)^n \frac{lM^n}{d^{3n+1}} \int_0^l e^{\frac{-Q}{RT_x}} \, dx \quad (20)$$

where T_x is the temperature at position x.

The ratio of the strain rates $\dot{\gamma}_1$, $\dot{\gamma}_2$ at different positions 1 and 2 in the specimen under a given torque can be obtained directly from Eq. (16) as

$$\frac{\dot{\gamma}_1}{\dot{\gamma}_2} = \left(\frac{d_2}{d_1}\right)^{3n} \quad (21)$$

or

$$\frac{\dot{\gamma}_1}{\dot{\gamma}_2} = e^{\frac{Q}{R}\left(\frac{1}{T_2} - \frac{1}{T_1}\right)} \quad (22)$$

for variations in diameter and temperature, respectively. For example, if there is a temperature gradient of 20 K over the length of the specimen at 1000 K and Q = 400 kJ mol^{-1}, then $\dot{\gamma}_1/\dot{\gamma}_2 = 2.7$.

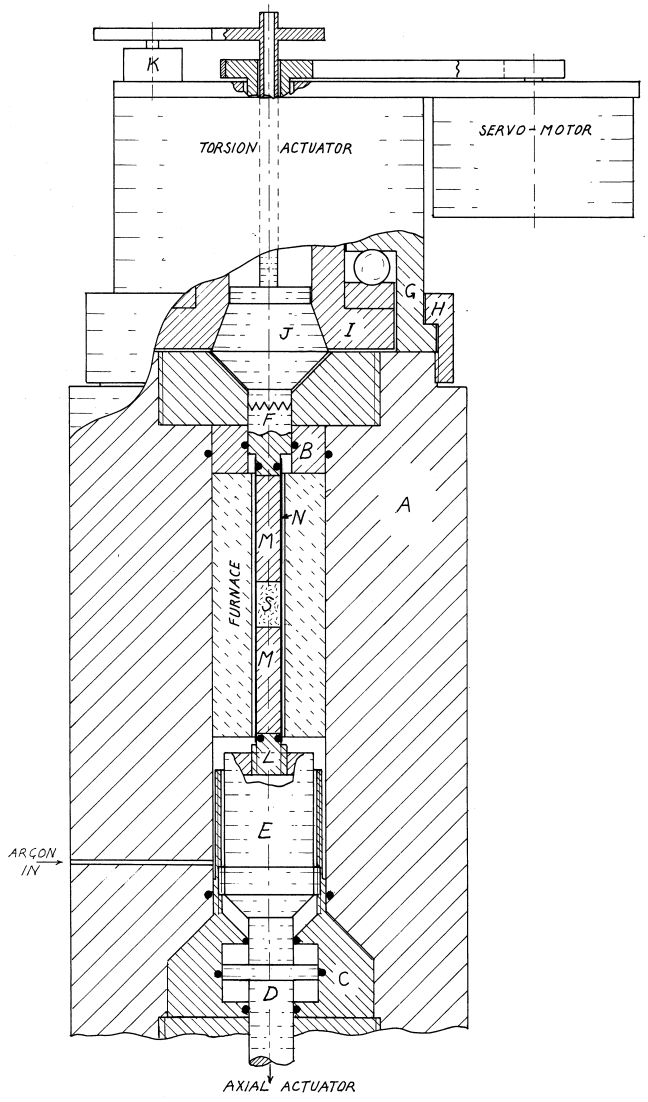

Fig. 5. Schematic diagram of high-pressure high-temperature testing machine with torsion actuator and specimen assembly.

3. Apparatus details

3.1. Apparatus configuration

The specific torsion system described here has been designed as an add-on feature for the Paterson gas-medium HPT testing machine (Paterson, 1990) but the principles are of general application. The environmental conditions are generally within the range of confining pressure to 500 MPa and temperature to 1600 K.

The basic layout of the system is shown in Fig. 5. The testing assembly is mounted in a vertically oriented pressure vessel A, with upper and lower closures B and C through which the torque and axial force can be transmitted to the specimen assembly from externally mounted actuators. The axial actuator is mounted below the pressure vessel and the axial force transmitted to the specimen assembly through the piston D and the internal load cell E. The torsion actuator is mounted at the top of the pressure vessel, its body G being attached to the top of the pressure vessel by an annular nut H which allows its removal for specimen insertion. The upper end of the specimen assembly consists of a boss F that projects through the closure and engages with the driver J seated in the rotating member I supported by a thrust bearing. The member I is connected to a servomotor drive through reduction gearing of 54,600:1 ratio. Operating the servomotor drive over a speed range from 3000 rpm (50 Hz) down to 0.03 rpm (5×10^{-4} Hz) gives a range of twist rate from 10^{-3} to 10^{-8} radians per second.

Since the machine is normally operated at elevated confining pressure, this aspect is used for the gripping of the various components. The friction associated with the large contact forces generated by the confining pressure acting on the boss F and on the bottom closure C ensures that the actuator body and the bottom plug do not rotate during a test, and the confining pressure also provides the means of gripping the driver J and the specimen assembly. The torque reaction at the bottom end of the specimen assembly is provided, first, by spines between the bottom specimen anvil and the load cell and, second, by spines between the internal load cell and the bottom closure. The latter spines permit the specimen assembly to be subjected to simultaneous axial and torsional loading. The minimum confining pressure for effective operation of the system is around 20–50 MPa, depending on the magnitude of torque to be applied.

The torsion driver J has a stem that projects out of the actuator and engages with a rotary displacement transducer K to register directly the twist of the speci-

men assembly with a rotary displacement transducer. Primary measurement of torque is done with the internal load cell E; the axial and torsional distortions of its elastic element under axial load and torque, respectively, are measured with displacement sensors (capacitance gauges, electric resistance strain gauges or LVDTs). Strain gauges are mounted on the boss of the driver J, which engages with the specimen assembly boss F, and also provide external torque measurement for an approximate indication of the torque, which includes the friction. The rating of the torsion actuator and internal torque cell is typically 1000 N m.

3.2. Specimen assembly

The simplest specimen assembly is indicated in Fig. 5. In this assembly the cylindrical specimen S is placed within the jacket N, flanked with two pistons M of the same diameter, normally of ceramic for high temperature tests. The two endpieces F and L are sealed within the jacket with O-rings. The seals are located outside the furnace and are at low temperature. In this specimen assembly, the torque is transmitted to the pistons and specimen by friction associated with the confining pressure, the jacket interior being vented to atmosphere at both ends. The maximum torque available for this arrangement is limited to that which would cause slip at any of the interfaces between specimen, pistons and endpieces. Assuming a coefficient of friction μ, the maximum torque transmitted across any interface can be obtained from the rigid-plastic Eq. (8) with $\tau_y = \mu p$ where p is the confining pressure. The corresponding maximum flow stress in a specimen undergoing homogeneous power-law creep can then be obtained by substituting this torque into the Eq. (10) to give

$$\tau = \frac{3 + \frac{1}{n}}{3} \mu p. \tag{23}$$

As an example, taking $\mu = 0.5$ for steel–ceramic or ceramic–rock interfaces and $p = 300$ MPa gives $\tau = 200$ MPa for $n = 1$ and $\tau = 164$ MPa for $n = 3$ as the maximum shear strength of a material that can be deformed in this way. The corresponding torque is 133 N m for a 15-mm specimen diameter.

If the frictional gripping of a plain cylindrical specimen is inadequate, alternative arrangements within the specimen assembly will be necessary, such as keying the components together or using a 'dog-bone' specimen, with appropriate jacketing. Thus, reducing the specimen diameter in the 'dog-bone' from 15 mm to 10 mm and swaging the jacket down over the specimen would increase the stress range by a factor of 3.4 (Eq. (10) and Fig. 4).

Although copper jackets can be used at relatively low temperatures, their high thermal conductivity tends to distort the temperature profile in the hot zone of the furnace and to overheat the O-ring seals. Thus iron jackets are more suitable at most temperatures, especially above 1000 K. In practice, jackets can show remarkable ductility, for example, a shear strain of about 22 has been reached in a test on Solnhofen limestone in an iron jacket at 1000 K. The choice of suitable jacket material for specific cases is an essential part of the experimental design.

In cases where it is desirable to have a nearly uniform stress state, hollow specimens can be considered, for which it is then necessary to jacket the inside diameter as well as the outside and to ensure that both are exposed to the confining pressure. However, in order to achieve a high degree of uniformity of stress, a thin-walled specimen is required, which poses problems of specimen preparation and handling because of fragility at atmospheric pressure. This question is considered further below in Section 5.

3.3. Control and conduct of experiments

Torsion tests can be carried out under displacement control or torque control, similar to the controls used in axial tests. Since the diameter of the specimen does not change during deformation, unless there is a change of volume, it is sufficient to control at constant motor speed or at constant torque in order to ensure constant strain rate or constant stress, respectively. For this purpose, feedback from a speed transducer on the motor or from the internal torque cell, respectively, is used. Relaxation experiments can be carried out simply by stopping the motor.

The strain rates in experiments can be influenced both by choice of twist rates and by choice of specimen dimensions, through $\dot{\theta} = (2l/d)\dot{\gamma}$. For example, for a specimen of 15 mm diameter and 10 mm length, the drive speed range of 10^{-3}–10^{-8} radians per second give a strain rate range 0.8×10^{-3} s^{-1}–0.8×10^{-8} s^{-1}. For more slender specimens, the same drive speed range gives lower strain rates, while the reverse applies for relatively short specimens, thus providing at least an extra order of magnitude in range of strain rates. The slender specimens might be used when exploring shear instabilities; the practical limitations are set by specimen fragility, relative jacket thickness and hot zone length to, say, 5 mm diameter and 30 mm length. The relatively short specimens allow the highest strains to be explored in given time; practical limitations are set mainly by grain size to, say, 15 mm diameter and 1 mm length. In this way the strain rate range available becomes 10^{-2}–10^{-9} s^{-1}.

The time required for reaching a given strain γ_{max} is given by $\gamma_{max}/\dot{\gamma}$. For example, if $\gamma_{max} = 10$ and $\dot{\gamma} = 10^{-5}$ s^{-1}, then the duration of the experiment is

10^6 s or nearly 12 days. Thus it is seen that considerable compromise may be called for between requirements for low strain rates and for large strains (geological strains at geological strain rates require geological time). However, for a given instantaneous microstructural state of the specimen, stress or strain-rate stepping can be used in exploring the corresponding rheology down to very low strain rates. Similar information can be obtained from relaxation experiments, which can be carried out simply by stopping the drive motor and monitoring the decay of the torque.

In carrying out or interpreting a torsion test using an internal load cell that measures both axial load and torque it is important to be aware of the effects of friction between the end of the specimen column L and the load cell E (Fig. 5). Thus, when establishing the axial load zero and axial touch point, it is important to ensure that no torque is being applied; otherwise, a large hysteresis will be found, originating in the friction at the torsional contact with the load cell. Conversely, when establishing the torque zero and torsional touch point, it is important to ensure that no axial load is being applied, for similar reasons. During the torsion test, even when the specimen column is positioned to be away from the axial touch point, the frictional contact in the splines will allow change in length of the specimen column to be reflected in change in the axial load signal, up to the limit set by frictional sliding; such an effect may arise from changes in pressure or temperature affecting the length of the column, as well as from changes in length of the specimen itself, such as that arising from dilatancy. These interactions may give a misleading impression of 'cross-talk' between axial and torsional load signals whereas in fact they represent real behaviour of the experimental assemblage, which in turn makes detection of 'cross-talk' within the load cell difficult to establish unambiguously.

Care also needs to be taken in interpreting the data from an experiment in which non-coaxial deformation occurs, such as 'dog-legging' (non-alignment of the ends of the specimen) or development of a 'bent' shape. An indication of whether 'dog-legging' is developing can often be obtained during the experiment by unloading the specimen and checking the 'touch-point' in both senses of twisting. If the internally measured torque zero is different in the two senses, indicating significant friction, then the specimen assembly may be exerting a lateral load on the load cell. A lateral load on the load cell may also cause some error in the torque signal due to incomplete compensation for side load. Therefore, particular caution should apply to rheological conclusions drawn from specimens that develop a non-cylindrical shape during deformation.

3.4. Calibration

The calibration of the torsional *displacement transducer* will usually be available from the manufacturer. Alternatively, a calibration may be derived from counting of complete revolutions of either the displacement transducer or of the motor. This step ensures that the values of θ are calibrated values in the following procedure.

The calibration of the *internal torque cell* is done under pressure. In order to allow for apparatus distortion, this calibration can be done by measurements in the elastic range on two steel bars of different diameters. Eq. (3) gives the elastic compliance of a given bar as

$$\frac{\theta}{M} = \frac{32l}{\pi G d^4} \tag{24}$$

where l and d are the length and diameter, respectively, of the calibrating bar and G is its shear modulus (around 83 GPa, depending somewhat on the specific steel).

Fig. 6(a) shows the relationships between the indicated values of torque, designated M', and the twist θ for the two bars, designated by subscripts 1 and 2, as well as, notionally, for a rigid bar (the notional twist θ_{app} for a 'rigid bar' represents the apparatus distortion outside of the calibrating bars and need not be linear with M'). The actual compliance of bar 1 will be

$$\frac{\theta_1 - \theta_{app}}{M} = \frac{32l_1}{\pi G d_1^4} \tag{25}$$

and that of bar 2

$$\frac{\theta_2 - \theta_{app}}{M} = \frac{32l_2}{\pi G d_2^4}. \tag{26}$$

Taking the difference and re-arranging gives

$$M = \frac{\pi G(\theta_1 - \theta_2)}{32\left(\frac{l_1}{d_1^4} - \frac{l_2}{d_2^4}\right)}. \tag{27}$$

Thus measurements of the twists θ_1 and θ_2 at a number of indicated torque values M' (Fig. 6b) enable a calibration curve for the torque M to be derived (Fig. 6c). In practice, it is convenient if this curve is linear but it is not necessarily so, and it may show some pressure dependence. The apparatus compliance $C = \theta_{app}/M$ (which excludes the compliance of the specimen assembly pistons) can also be obtained from Eqs. (25) and (26). A typical value of this compliance is 4×10^{-5} radians per N m at 300 MPa confining pressure for the apparatus discussed here.

Finally it is necessary to make a correction to the measured torque for the torque supported by the jacket on the specimen. If the flow stress for axial deformation of the jacket material is known from direct measurement or taken from a flow law such as that of Frost and Ashby (1982), the flow stress in shear can be calculated assuming the von Mises failure criterion. If not, a calibration must be carried out. This is most readily done using a specimen of the same material as the jacket and calculating the torque supported by the jacket using relationships appropriate to power-law rheology if the behaviour is of this type. An alternative is to use a hollow specimen assembly without specimen, spinning the outer jacket down to fit over the inner jacket and measuring the diameters after pressurising to eliminate any gap. The magnitude of the correction is of the order of 5% for a 15-mm-diameter specimen in a jacket of 0.25 mm wall thickness when the jacket material is of similar strength to the specimen.

4. Analysis of experiments—microstructural

The microstructural study of the specimens from torsion tests is more complex than for axial deformation tests because of the gradient in strain rate and strain with radius. There are three principal ways of cutting sections for microscopical examination, shown in Fig. 7, which can be referred to as 'longitudinal tangential', 'longitudinal axial' and 'transverse'. These sections have the following specific characteristics:

Longitudinal tangential: the transport direction is approximately parallel to the section (analogous to the *xz* plane of Ramsay, 1980) and normal to the longitudinal dimension, provided the section is cut close to the surface. Strain localisation effects should be revealed by variations in strain in the direction of the longitudinal dimension. In the absence of localisation, the strain and strain rate are approximately uniform within this section. This section is normally the most informative because of the orientation and of the relatively large area at maximum strain.

Longitudinal axial: the shear transport direction is normal to the section (analogous to a section of a shear zone normal to the transport direction, or the *yz* plane of Ramsay, 1980) and the strain and strain rate increase in the normal direction from the specimen axis which lies in the section. Strain localisation effects should be revealed within this section by variations parallel to the longitudinal dimension.

Transverse: the shear displacement or transport direction lies in the plane of the section (analogous to that in a section parallel to a shear zone, or the *xy* plane of Ramsay, 1980), and the strain and strain rate increase radially from the centre, with radial symmetry in homogeneous and isotropic material. Strain localis-

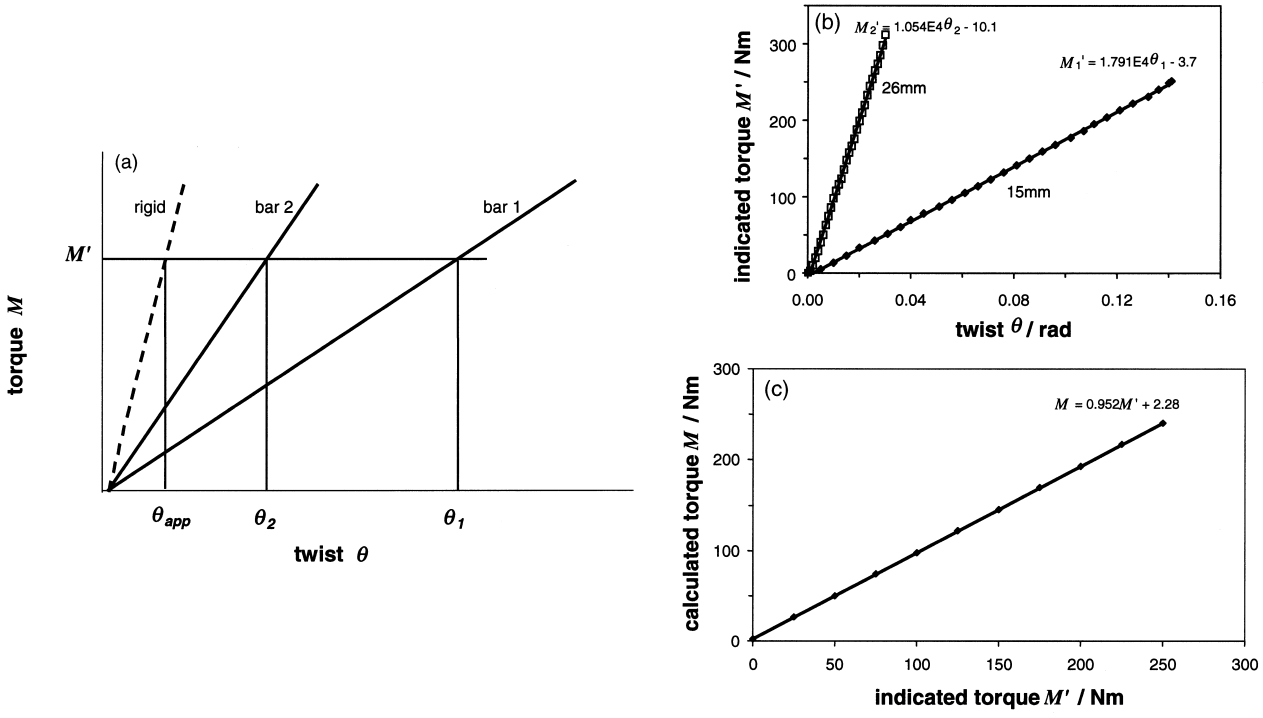

Fig. 6. Torque calibration procedure. (a) Schematic relationship between twist and indicated torque for two bars of different diameter. (b) An example of calibration data. (c) Calibration curve derived from data in (b).

ation effects can only be studied by cutting successive sections along the specimen axis.

In the interpretation of variations in radial and axial directions, respectively, it cannot be assumed that the variations in the transverse and longitudinal sections can be entirely attributed to the variation in the strain itself because the strain rate is varying also. To separate the effects of these two factors, experiments at different twist rates are required.

The nature of the microstructural studies will, of course, depend on the aims of the research. The studies are likely to include observations of recrystallisation, grain-size and shape, and other microscopical features, observations on lattice and shape preferred orientations, and electron microscopical observations on dislocations, grain boundary structures, etc.

Variations in observed structure with position in the specimen must be interpreted with care because of the complex interrelationships between strain, strain rate and structural evolution. Thus, if the achievement of a steady-state torque–twist relationship means that a steady-state stress–strain condition has been achieved at each radius, the corresponding microstructure is not necessarily homogeneous because the local steady state at each radius may correspond to a different grain size in dynamic recrystallisation, leading to a radial variation in grain-size in the specimen. Conversely, the observation of a gradient in grain-size in a transverse or longitudinal section does not necessarily mean that the specimen is not deforming in a steady state in a single rheological regime.

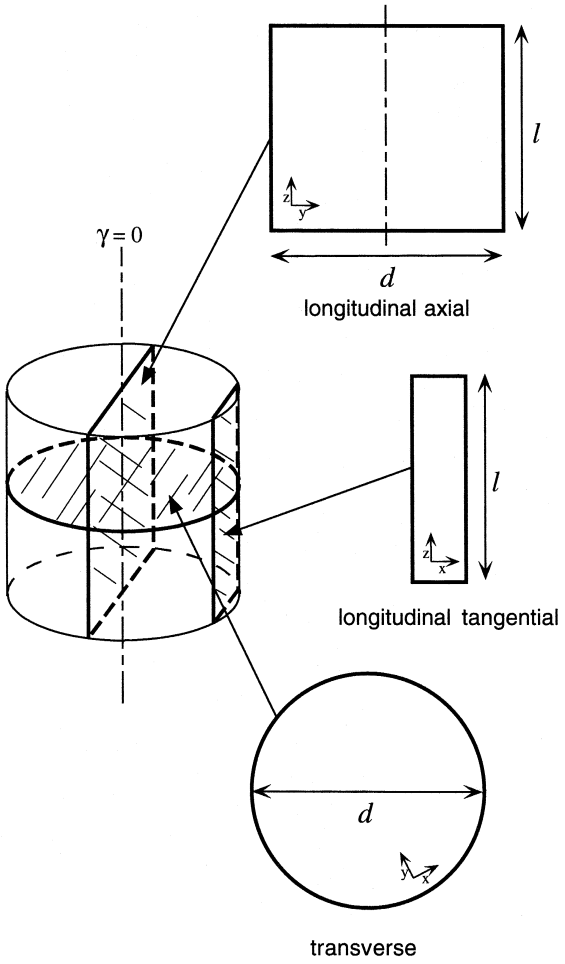

Fig. 7. Schematic diagram showing the three principal ways of cutting sections.

5. Analysis of experiments—rheological

Torsion experiments carried out to large strains give a broader view of the effects of strain history on the flow stress than do conventional axial deformation experiments. Thus, gradual changes in microstructure such as the development of crystallographic preferred orientation or change in grain-size through recrystallization can result in gradual changes in flow stress at a given strain rate over a large range of strain. At any particular stage in the strain history, the maximum strain rate at the surface of the specimen is given by Eq. (4), and the flow stress at this strain rate is given by Eq. (10), assuming that the strain rate dependence within the specimen can be represented by a power law. Stepping tests then enable the strain rate and temperature dependencies and the pre-exponential factor for the current flow stress to be determined using Eqs. (12)–(14). The values of the parameters thus determined may be useful in constraining deductions about possible deformation mechanisms at a particular stage in the deformation. However, their usefulness for extrapolating the rheological behaviour to geological conditions will depend on the degree to which a 'steady-state' or strain-independent behaviour can be defined.

The procedures just outlined represent the primary approach to determining the rheological parameters. However, the stress exponent can also be obtained from relaxation experiments if these are carried out under well-defined conditions. In such tests, with the actuator drive stationary, the torque relaxation rate at a given torque is used to estimate the strain rate at the corresponding stress, through the relationship

$$\dot{\theta} = C\dot{M} \tag{28}$$

where $\dot{\theta}$ is the twist rate in the specimen at the torque M at which the torque relaxation rate $\dot{M}$ is measured, and C is the elastic compliance of the torque loading system (see Section 3.4 above). Then, using Eq. (12) we have

$$n = \frac{\mathrm{d}\ln\dot{\theta}}{\mathrm{d}M} = \frac{\mathrm{d}\ln\dot{M}}{\mathrm{d}M} + \frac{\mathrm{d}\ln C}{\mathrm{d}M}. \quad (29)$$

If the machine is behaving with constant compliance, then

$$n = \frac{\mathrm{d}\ln\dot{M}}{\mathrm{d}M} = \frac{1}{\dot{M}}\frac{\mathrm{d}\dot{M}}{\mathrm{d}M} \quad (30)$$

at each stage in the relaxation.

It should be emphasised that the Eqs. (12)–(14) and (30) are only strictly applicable if the material deforms throughout the specimen according to the same creep law, that is, with the same A, n and Q values at all stresses and strain rates below the maxima at the surface. This assumption will not be valid if the rock undergoes a rheological transition with decreasing stress and strain rate below those applying at the surface of the specimen. However, because of the cubic dependence of the torque on the diameter, a large proportion of the measured torque relates to an outer fraction of the radius that is relatively small, and hence relates to stresses near the maximum stress. Thus, for $n=3$, Eqs. (10) and (11) can be used to show that 90% of the torque comes from the outer half of the radius, across which the stress is within 20% of the maximum stress (Fig. 3). Eqs. (12)–(14) and (30) can therefore be used as a good approximation for determining n and Q provided that there is not a rheological transition close below the maximum stress. Even if the latter conditions are not fulfilled, twist-rate or torque stepping tests would probably give a good qualitative indication of the presence of a transition.

In principle, the use of hollow specimens would overcome the limitations of radially inhomogeneous behaviour in solid specimens. For power-law creep, the ratio of shear stress at the inside diameter τ_i to that at the outside diameter τ_o is given by

$$\frac{\tau_i}{\tau_o} = \left(\frac{d_i}{d_o}\right)^{\frac{1}{n}} \quad (31)$$

A robust specimen of 22 mm outside diameter and 16 mm inside diameter has a stress ratio of 0.90 for $n=3$ (Fig. 3). If it is desired to have a stress ratio of 0.95, for example, the inside diameter would have to be 19 mm, giving a wall thickness of 1.5 mm. For $n=1$, the requirement on wall thickness for high stress ratio is even more stringent, and probably impractical for many materials. Thus, in view of the point made in the previous paragraph that the major part of the torque relates to the outer radii of the specimen and because the torque supported by the jacketing will be nearly double that for a solid specimen, it will often be questionable whether the extra experimental difficulties in using hollow specimens are worth the inconvenience for the sake of marginal improvement in rheological analysis.

An alternative procedure for dealing with radially inhomogeneous behaviour is to make measurements on two specimens of the same material with slightly different diameters d_1 and d_2 ($d_1 > d_2$) and take the difference in the torques, corrected slightly for the difference in torque supported by the two jackets, as being the torque supported by a hollow specimen of outer diameter d_1 and inner diameter d_2. In this case, if we insert $d_2/2$ and $d_1/2$ as the integration limits in Eq. (5) and assume power-law rheology with a unique n for the material between d_2 and d_1 in the larger specimen, so that $\tau_r = (2r/d_1)^{1/n}\tau$ as in the derivation of Eq. (10), it follows that

$$\Delta M = M_1 - M_2 = \frac{\pi\tau}{4\left(3+\frac{1}{n}\right)}\left(\frac{d_1^{3+\frac{1}{n}} - d_2^{3+\frac{1}{n}}}{d_1^{\frac{1}{n}}}\right) \quad (32)$$

in analogy with Eq. (11). The relations Eqs. (12)–(14) and (30) can then be applied to ΔM to obtain the rheological parameters n, Q and A that apply to the layer between d_1 and d_2.

Further insight into the rheological analysis can be obtained from more detailed consideration of rheological regime maps and the actual stress–strain relationships that might be expected for homogeneous behaviour, as follows:

First, consider the rheological regime map of Fig. 8,

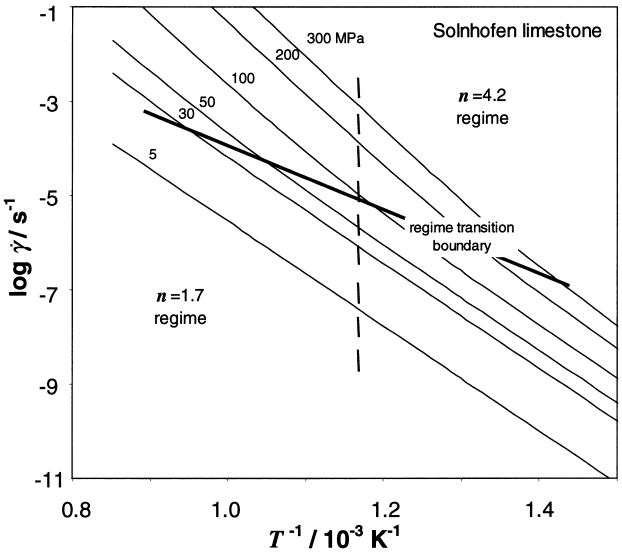

Fig. 8. Rheological regime map for Solnhofen limestone based on Schmid et al. (1977); the contours for the shear stresses marked have been obtained by adding the flow laws defined for the two regimes. The short vertical lines represent the range of strain rates for the outer half of the radius of a specimen, from which the measured torque in a torsion test essentially derives. T = temperature, $\dot{\gamma}$ = shear strain rate.

based on flow laws derived from the measurements of Schmid et al. (1977) for Solnhofen limestone. The span of log strain rates in the outer half of the radius of a specimen is $\log 0.5 = -0.301$, or slightly less than one third of a decade of log strain rate. Several such spans are marked (vertical lines) for a decreasing series of torque values at a temperature of 900 K. It is seen that the span of stresses contributing most of the torque generally falls entirely within one regime field; only over a relatively small torque range does it fall across the regime boundary. Moreover, this boundary is not very sharp in practice. Thus the use of rheological data derived from solid specimens should fairly well define the regime fields and give reliable rheological parameters.

Second, consider hypothetical stress–strain curves for a series of constant strain rates at a given temperature. Fig. 9(a) depicts a case in which steady state is soon reached and maintained to large strains. The dashed curves represent the stress distributions within specimens for several maximum (surface) strains. The weighted integration of these stresses according to Eq. (5) gives the torque–twist curve of Fig. 9(b). Fig. 10(a) depicts a case in which a strain softening is followed by steady state behaviour. A similar analysis leads to the torque–twist curve of Fig. 10(b). These examples show that, while the stress–strain history is qualitatively reflected in the torque–twist curves, the details are less distinct.

There may be situations in which the microstructure can give guidance to the rheological analysis. Thus, if, for example, due to dynamic recrystallisation at the higher strain rates and strains, the specimen were to develop a fine-grained outer rim between radius r_i and the surface radius r_o, which did not develop in the inner parts of the specimen, the specimen could be treated as consisting of two concentric parts and the integration in Eq. (5) could be carried out separately for the two respective ranges and added, according to

$$M = 2\pi \int_0^{r_i} \tau_r r^2 \, \mathrm{d}r + 2\pi \int_{r_i}^{r_o} \tau_r r^2 \, \mathrm{d}r. \tag{33}$$

If the rheological parameters can be assumed to be known for one of the zones (for example, the unrecrystallised zone), the corresponding integral could be eval-

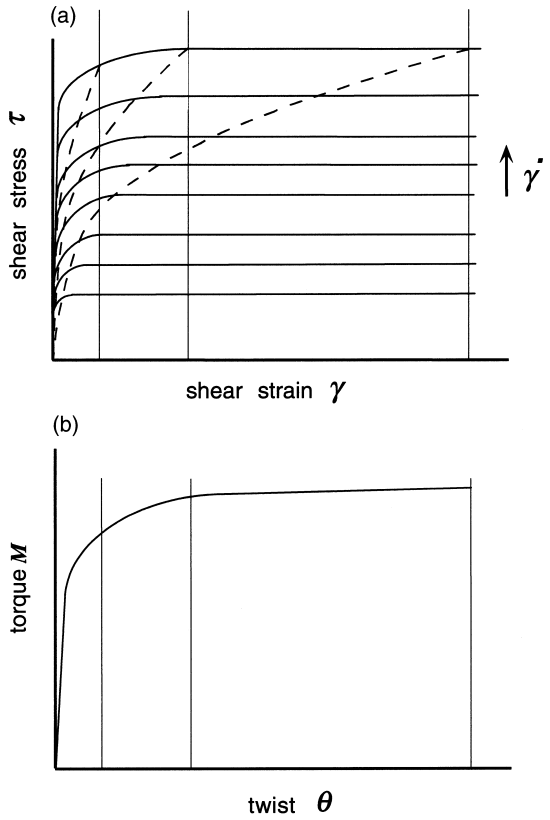

Fig. 9. Derivation of torque–twist curve from shear stress–shear strain relationships for a case of early approach to steady state. (a) Hypothetical shear stress–shear strain curves for a series of strain rates. The dashed lines represent examples of the distributions of stress within specimens strained to the maximum shear strain represented by the vertical lines. (b) Torque–twist curve derived using Eq. (5).

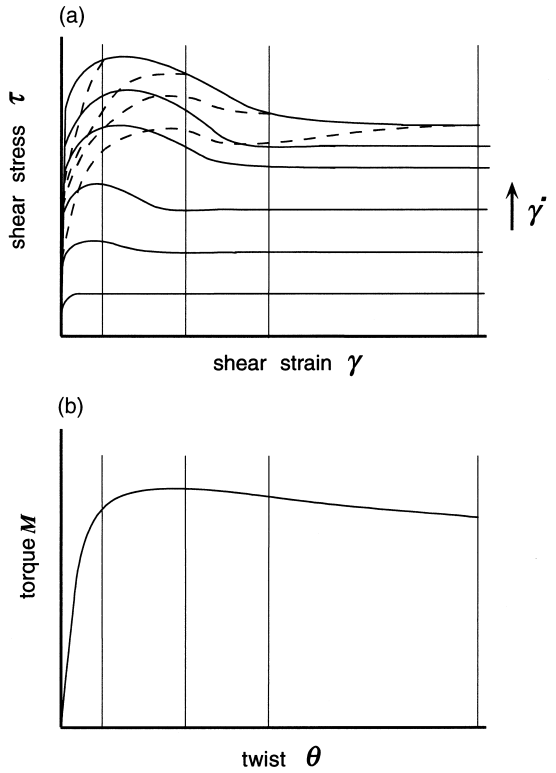

Fig. 10. Derivation of torque–twist curve from shear stress–shear strain relationships for a case involving strain softening. (a) Hypothetical shear stress–shear strain curves for a series of strain rates. The dashed lines represent examples of the distributions of stress within specimens strained to the maximum shear strain represented by the vertical lines. (b) Torque–twist curve derived using Eq. (5).

uated and subtracted from M, to give a value for the integral relating to the other zone, and thus facilitate further analysis of its rheological properties.

6. Other aspects of torsion tests

So far no account has been taken of any role of non-zero strain or stress in the axial direction. There are two such situations that may be mentioned here.

To a first approximation, no change in length of a specimen undergoing torsional deformation would be expected for an initially homogeneous and isotropic material deforming at constant volume. However, small changes in length have often been observed in metals (Van Arsdale et al., 1980; Tóth et al., 1992; Jonas, 1993) and might be similarly expected in rocks, especially since volume change may occur due to microcracking or phase change. Length changes can be monitored with the axial displacement transducer if a small axial load is applied to the specimen and maintained constant. No careful measurements have yet been made of length changes in rocks.

The second application where axial effects come into consideration is in the determination of the role of all three principal stresses in the rheology. The use of combined torsion and axial tests on hollow cylinders has been a classic method for determining the constitutive laws for plastic deformation of metals. Similar application can be expected for determining the full rheology of rocks, especially taking dilatancy into account.

A knowledge of the constitutive law is a prerequisite to comparing axial and torsion test results. It has often been assumed that a von Mises type of constitutive relationship will apply in creep deformation of rocks (Odqvist, 1935, 1966). In this case, under general states of stress, comparable flow rates would be expected at identical values of the von Mises equivalent stress

$$\sigma_{\text{eff}} = \sqrt{\frac{1}{2}\left\{(\sigma_1 - \sigma_2)^2 + (\sigma_2 - \sigma_3)^2 + (\sigma_3 - \sigma_1)^2\right\}} \tag{34}$$

in which σ_1, σ_2, σ_3 are the principal stresses. Then, since the principal stresses in the torsion test are $p+\tau$, $p-\tau$, and p, and in the axial test are $\sigma+p$, p, and p, where p is the confining pressure, τ the shear stress determined with the internal torque cell in the torsion test, and $\sigma(=\sigma_1-\sigma_3)$ the axial stress determined with the internal load cell in the axial test, we have

$$\sigma_{\text{eff}} = \sigma \text{ in the axial test,} \tag{35}$$

and

$$\sigma_{\text{eff}} = \sqrt{3}\tau \text{ in the torsion test.} \tag{36}$$

In order to compare flow rates under the different states of stress, we use the equivalent strain rates

$$\dot{\varepsilon}_{\text{eff}} = \sqrt{\frac{2}{9}\left\{(\dot{\varepsilon}_1 - \dot{\varepsilon}_2)^2 + (\dot{\varepsilon}_2 - \dot{\varepsilon}_3)^2 + (\dot{\varepsilon}_3 - \dot{\varepsilon}_1)^2\right\}} \tag{37}$$

where $\dot{\varepsilon}_1$, $\dot{\varepsilon}_2$, $\dot{\varepsilon}_3$ are the principal strain rates. Putting $\dot{\varepsilon}_2 = \dot{\varepsilon}_3 = -\dot{\varepsilon}_1/2$ for the axial test and $\dot{\varepsilon}_2 = -\dot{\varepsilon}_3 = \dot{\gamma}/2$, $\dot{\varepsilon}_1 = 0$ for the torsion test ($\dot{\gamma}$ is the maximum engineering shear strain rate), we have

$$\dot{\varepsilon}_{\text{eff}} = \dot{\varepsilon}_1 \text{ in the axial test,} \tag{38}$$

$$\dot{\varepsilon}_{\text{eff}} = \frac{1}{\sqrt{3}}\dot{\gamma} \text{ in the torsion test.} \tag{39}$$

If we compare the flow stresses in axial and torsion tests at the same *equivalent* strain rates (and therefore the same equivalent stresses), then we would expect

$$\sigma = \sqrt{3}\tau \text{ or } \tau = \frac{1}{\sqrt{3}}\sigma. \tag{40}$$

However, if we compare the flow stresses in axial and torsion tests at the same *nominal* strain rate ($\dot{\varepsilon} = \dot{\gamma}$), then the equivalent strain rate in torsion will be $1/\sqrt{3}$ times that in the axial test and the equivalent stress will be lower by a factor that depends on the stress vs. strain rate relationship. If this relationship is a power law with stress exponent n, we would expect

$$\tau = \left(\frac{1}{\sqrt{3}}\sigma\right)\left(\frac{1}{\sqrt{3}}\right)^{\frac{1}{n}} = \frac{1}{3^{\frac{1+n}{2n}}}\sigma \tag{41}$$

or

$$\sigma = 3^{\frac{1+n}{2n}}\tau. \tag{42}$$

For Newtonian flow, $n = 1$, and Eq. (42) gives $\sigma = 3\tau$ and, for n = 3–5, Eq. (42) gives $\sigma \approx 2\tau$.

7. Examples of torsion tests to high strains

To illustrate the application of torsion testing, we first show that for Carrara marble it leads to rheologies and microstructures similar to those from more conventional tests at similar conditions (Table 2), and then show that significant new information is available because of the higher strains in torsion tests. Carrara marble has been chosen for such a comparison because considerable experimental data already exist showing the influence of strain on both microstructure and rheology and showing that high strains may be necessary before either reaches steady-state (e.g. Schmid et al., 1980, 1987; Rutter, 1974, 1995, 1998; Covey-Crump, 1994, 1997, 1998). Carrara marble is used for

Table 2
Compilation of rheological data for Carrara marble deformed at a temperature of 973 K, confining pressures of 200–300 MPa and shear strain rates of approximately 5×10^{-4} s^{-1}

Test type	Shear strain rate (s^{-1})[a]	Peak shear stress (MPa)[a]	Total shear strain (γ)[a]	Reference
Torsion	4.7×10^{-4}	57	0.52	This study
Torsion	4.7×10^{-4}	57	2.1	This study
Torsion	4.7×10^{-4}	66	7.0	This study
Stepping sequence #1[b]	4.7×10^{-4}	64	0.3–0.5	$n = 12.7 \pm 1.0$
Stepping sequence #2[b]	4.7×10^{-4}	60	3.06–4.0	$n = 7.7 \pm 1.0$
Stepping sequence #3[b]	4.8×10^{-4}	58	5.35–6.0	$n = 7.3 \pm 0.5$
Split-cylinder shear	4.7×10^{-4}	72	2.85	Schmid et al., 1987
Coaxial compression	17×10^{-4}	66	> 0.2	Schmid et al., 1980
Coaxial compression	1.9×10^{-4}	60	> 0.2	Schmid et al., 1980
Coaxial compression	2.9×10^{-4}	64	0.88	Rutter, 1995
Coaxial compression	3.8×10^{-4}	70	0.52	Covey-Crump, 1998
Coaxial extension	4×10^{-4}	82	1.4	Rutter, 1995
Flow law (Regime 2)	4.7×10^{-4}	69	–	Schmid et al., 1980

[a] For the torsion tests, values of strain, strain rate, and stress were calculated from Eqs. (3), (4) and (10). For coaxial tests, the shear values were calculated from the coaxial values using Eqs. (38) and (39).

[b] Strain-rate stepping tests used to estimate n-values. The listed strain rates and stresses are those at the beginning of the stepping sequence. Strain rates for a sequence were $1.0\times$, $0.33\times$, $0.10\times$ and $1.0\times$ the listed value. The complete stepping sequence occurred over the listed range of shear strain (Fig. 11). The uncertainty in the n-value represents the maximum range determined in the strain-rate stepping sequence.

deformation experiments because it is homogeneous, medium-grained and almost pure calcite.

Our test specimens were of the Lorano Bianco Carrara marble that has been widely distributed for inter-laboratory comparison. Specimens of 15 mm diameter and 10 mm length were cored parallel to the A-orientation (Pieri et al., 2000a) and jacketed in iron (0.2 mm wall thickness). Tests were carried out at 973 K, strain rate 4.7×10^{-4} s^{-1} and confining pressure 300 MPa, up to shear strains $\gamma = 7$. Flow can be described by a power-law with a high stress exponent ($n \geq 7$). The resulting stress–strain curves are compared with previously published curves from other types of tests in Fig. 11. In all cases, the shear stresses reached similar values for $\gamma = 0.2$ and thereafter appeared to remain approximately constant up to $\gamma = 1$ (Fig. 11a). However, when a greater strain range is considered, noticeable work softening is evident (Fig. 11b). At three points during the $\gamma = 7$ test, strain-rate stepping was performed to determine the evolution of the stress exponent n with strain (Fig. 11b). The value of n decreased from 13 for $\gamma = 0.5$ to approximately 7 for $\gamma = 3.5$, and remained constant to $\gamma = 7$. This change in n suggests an evolution in deformation mechanism.

Ultra-thin (≤ 10 μm) sections were made of the starting material and of the specimen strained to $\gamma = 2.1$ in the orientations depicted in Fig. 7. The starting material has a unimodal grain size distribution and a mean grain size of 140 μm (Fig. 12a). Most grains are equant in shape and contain thin randomly oriented twin lamellae, serrate grain boundaries, and a faint undulatory extinction. There is also a weak

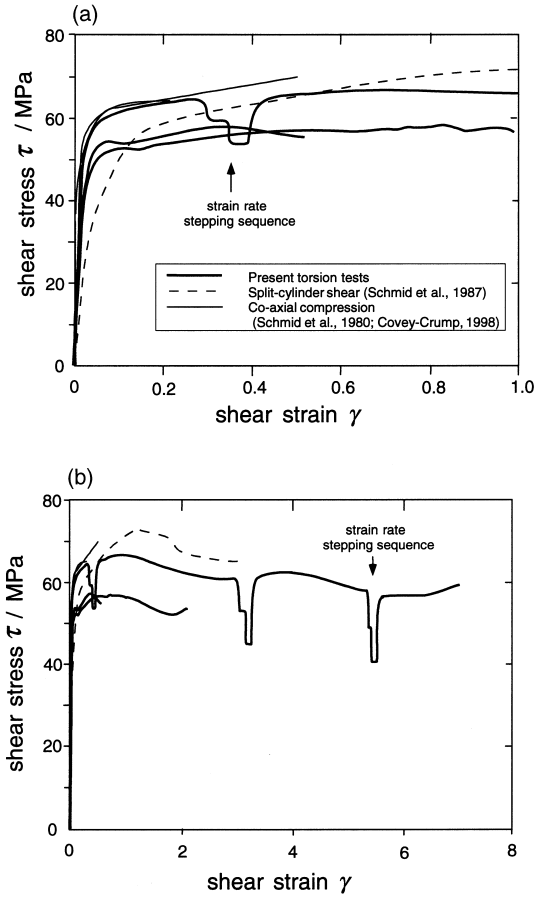

Fig. 11. Shear stress–strain curves for Carrara marble at 973 K and 200–300 MPa (see Table 2). (a) Low-strain region. (b) High-strain region.

grain-shape fabric and a weak crystallographic preferred orientation. This microstructure is similar to that described by others (e.g. Schmid et al., 1980; Rutter, 1995; Covey-Crump, 1998).

Examples of microstructures from the sheared specimen are shown in Fig. 12(b–f). The longitudinal tangential section shows a grain shape change that corresponds approximately to the finite strain (Fig. 12b). Many grains contain strong undulatory extinction, thick-bowed twins, and subgrains, all in-

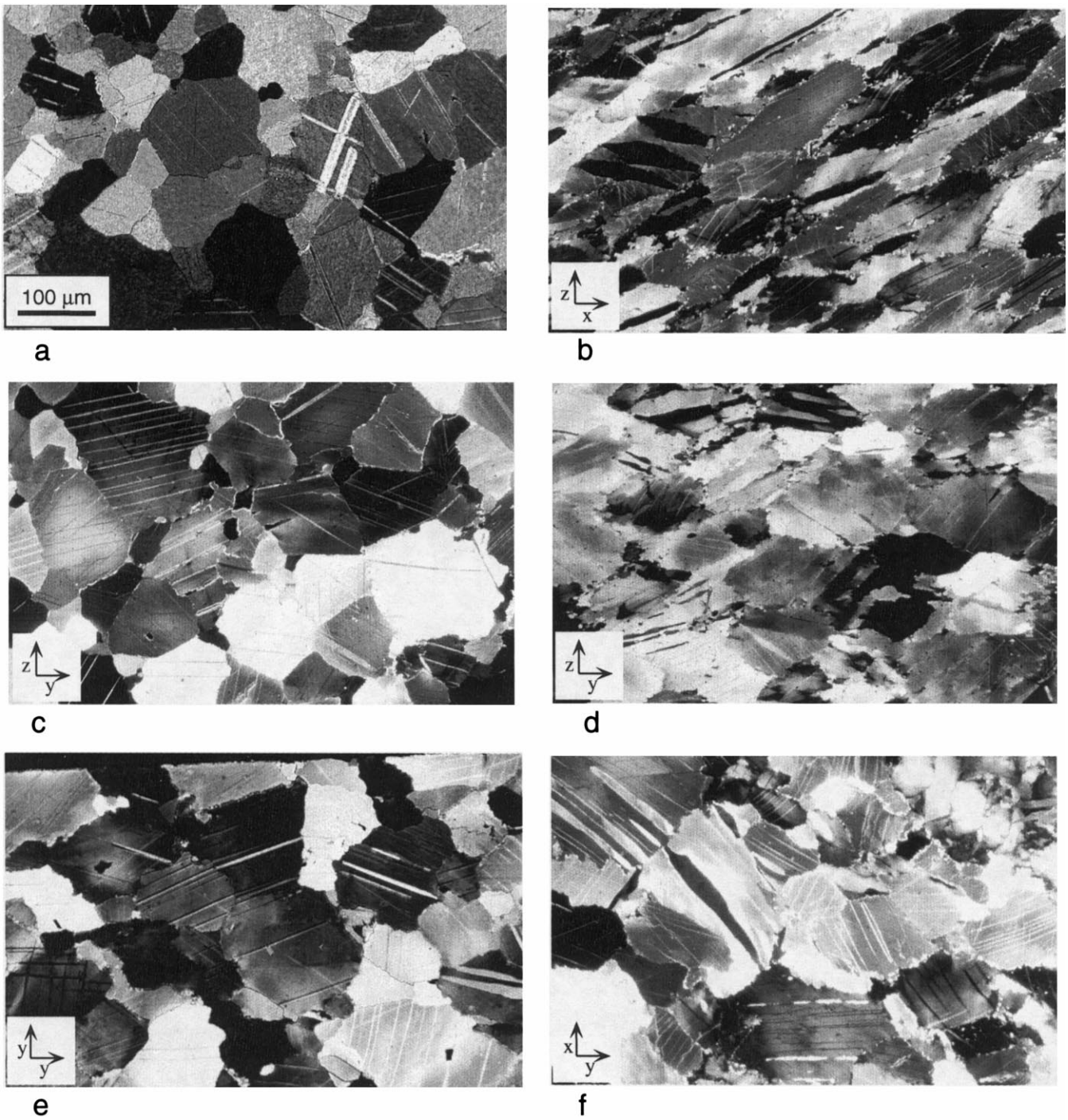

Fig. 12. Microstructures of Carrara marble. (a) Undeformed. (b) Longitudinal tangential section, $\gamma = 2$. (c) Longitudinal axial section from near centre of specimen ($\gamma \approx 0$). (d) Longitudinal axial section near outer edge of specimen (specimen boundary is on the right-hand side). (e) Transverse section from near centre of specimen ($\gamma \approx 0$). (f) Transverse section near outer edge of specimen (specimen boundary is on the right-hand side). All micrographs are to the same scale as shown in (a).

dicative of dislocation glide and climb. There is also abundant evidence for incipient dynamic recrystallisation on grain boundaries, in pockets within the large grains, and in some twin bands. These microstructures are similar to those seen in the direct shear tests of Schmid et al. (1987), deformed at similar conditions. In thin sections of the longitudinal axial and transverse orientations, the microstructures continuously evolve from the undeformed cylinder core (Fig. 12c and e) to the outer surface where γ is a maximum (Fig. 12d and f). In the core, the microstructure shows the static adjustments caused by annealing at 973 K for approximately 2 h, e.g. smoother grain boundaries and minor grain growth. Observations from such sections can be used to subtract the effects of temperature and time from the dynamic affects of strain and stress. At the high-strain outer edge of the longitudinal axial section (Fig. 12d) many microstructures are similar to those in the longitudinal tangential section (Fig. 12b), e.g. undulatory extinction, twins, and recrystallised grains. The grains have undergone an apparent shortening in both the x- and z-directions (seen in transverse and longitudinal axial sections, respectively). Assuming plane strain, the mean grain-size in the neutral y-direction compared to that near the central axis gives a measure of strain-induced grain growth or grain-size reduction.

The rheological and microstructural data collected for several rock types using the new torsion apparatus illustrate the importance of carrying deformation experiments to very high strains in order to throw light on geological behaviour in shear zones. The following are such examples:

1. The study of Casey et al. (1998) on Solnhofen limestone using electron back-scattering diffraction (EBSD) shows that a steady-state texture developed which persisted over a large range of strain, to at least $\gamma = 12$.
2. In Carrara marble, Kunze et al. (1998) and Pieri et al. (2000) have found evidence for the $(r) < a >$ slip system in high strain simple shear. This slip system was previously only seen in dolomite. Also in Carrara marble, Pieri et al. (2000) used large strain torsion tests to show that strain weakening in the dislocation creep field is associated with strong crystallographic preferred orientation and with dynamic recrystallisation to a finer grain-size.
3. Stretton and Olgaard (1997) showed that in torsion of anhydrite to large strain there is a reduction in grain-size due to dynamic recrystallisation, which is associated with marked strain weakening and a reduction in n value from 5 at the peak stress to 1 at large strain. It is concluded that dynamic recrystallisation leading to a reduction in grain-size can cause a transition from dislocation-controlled creep to diffusion-controlled creep.
4. Wendt et al. (1999) describe rheological and microstructural results of a high temperature, high strain torsion test on a silicate, a synthetic Ca-rich plagioclase aggregate deformed to $\gamma = 1$ at 1473 K. The sample deformed uniformly and developed strong grain shape and crystallographic preferred orientations.

8. Conclusions

The torsion test offers the following special features as a procedure for studying the rheological behaviour of rock specimens at high pressure and high temperature:

1. It allows the study of non-coaxial deformations and thus the simulation of the simple shear style of deformation commonly observed in naturally deformed rocks. The microstructures and textures resulting from such deformation can thus be established.
2. The effects of large strains can be explored without significantly changing the geometry of the specimens, thus revealing the influence of strain on the evolution of rheology, microstructure and crystallographic preferred orientation. In particular, the existence of steady-state deformation can be tested more thoroughly and the evolution of deformation mechanisms explored.
3. Torsion testing also opens up the possibility of exploring whether localisation develops during large strains and, if so, why.
4. By combining axial deformation with torsion, the effect of variation of all three principal stresses can be explored.

Some preliminary observations to high strains indicate that strain softening can be associated with either lattice rotations or dynamic recrystallisation.

Acknowledgements

The authors are grateful to the Geologisches Institut, ETH, Zürich, GeoForschingsZentrum Potsdam and Exxon Production Research Company for support during the writing of this paper and to their colleagues in these institutions (especially I. Stretton, M. Pieri, K. Kunze, J.-P. Burg, G. Dresen, E. Rybacki and M. Naumann) for stimulating discussions on torsion testing. They are also grateful to T. Shimamoto for review comments.

References

Blankenship, C.P., Larsen, M., Sutcliff, J.A., 1995. Deformation and fracture of Ni Al single crystals tested in torsion. Acta metallurgica et materialia 43, 1549–1558.

Boeker, R., 1915. Die Mechanik der bleibenden Formänderung in kristallinisch aufgebauten Körpern. Verein deutscher Ingenieure. Mitt. Forsch. 175, 1–51.

Bons, P.D., Urai, J.L., 1996. An apparatus to experimentally model the dynamics of ductile shear zones. Tectonophysics 256, 145–164.

Bouchez, J.L., Duval, P., 1982. The fabric of polycrystalline ice deformed in simple shear: experiments in torsion, natural deformation and geometrical interpretation. Textures and Microstructures 5, 171–190.

Bridgman, P.W., 1935. Effects of high shearing stress combined with high hydrostatic pressure. Physical Review 48, 825–847.

Bridgman, P.W., 1936. Shearing phenomena at high pressure of possible importance for geology. Journal of Geology 44, 653–669.

Canova, G.R., Shrivastava, S., Jonas, J.J., G'Sell, C., 1982. The use of torsion testing to assess material formability. In: Newby, J.R., Niemeier, B.A. (Eds.), Formability of Metallic Materials—2000 A.D. American Society for Testing and Materials, ASTM-STP 753, pp. 189–210.

Carter, N.L., Christie, J.M., Griggs, D.T., 1964. Experimental deformation and recrystallization of quartz. Journal of Geology 72, 687–733.

Casey, M., Kunze, K., Olgaard, D.L., 1998. Texture of Solnhofen limestone deformed to high strains in torsion. Journal of Structural Geology 20, 255–267.

Covey-Crump, S.J., 1994. The application of Hart's state variable description of inelastic deformation to Carrara marble at $T < 450°C$. Journal of Geophysical Research 99, 19793–19808.

Covey-Crump, S.J., 1997. The high temperature static recovery and recrystallization behaviour of cold-worked Carrara marble. Journal of Structural Geology 19, 225–241.

Covey-Crump, S.J., 1998. Evolution of mechanical state in Carrara marble during deformation at 400 to 700°C. Journal of Geophysical Research 103, 29781–29794.

Dell'Angelo, L.N., Tullis, J., 1996. Textural and mechanical evolution with progressive strain in experimentally deformed aplite. Tectonophysics 256, 57–82.

Dell'Angelo, L.N., Tullis, J., Yund, R.A., 1987. Transition from dislocation creep to melt-enhanced diffusion creep in fine-grained granitic aggregates. Tectonophysics 139, 325–332.

Durand, E., 1975. L'essai de torsion et la résistance au cisaillement des roches. Rock Mechanics 7, 199–230.

Durand, E., Comes, G., 1974. L'essai de torsion et la résistance au cisaillement des roches. In: Advances in Rock Mechanics: Proceedings of the Third Congress of the International Society for Rock Mechanics, Denver, Colorado, September 1–7, 1974. National Academy of Sciences, Washington, D.C, pp. 226–232.

Frost, H.J., Ashby, M.F., 1982. Deformation Mechanism Maps: The Plasticity and Creep of Metals and Ceramics. Pergamon, Oxford.

Handin, J., Heard, H.C., Magouirk, J.N., 1967. Effects of the intermediate principal stress on the failure of limestone, dolomite, and glass at different temperatures and strain rates. Journal of Geophysical Research 72, 611–640.

Handin, J., Higgs, D.V., O'Brien, J.K., 1960. Torsion of Yule marble under confining pressure. In: Griggs, D., Handin, J. (Eds.), Rock Deformation, Geological Society of America Memoir, 79, pp. 245–274.

Hardwick, D., Tegart, W.J.G. McG., 1961. La déformation des métaux et alliages par torsion à haute température. Memoires scientifiques de la revue de metallurgie LVIII, 869–880.

Hobbs, B.E., Means, W.D., Williams, P.F., 1976. An Outline of Structural Geology. John Wiley, New York.

Jessell, M.W., Lister, G.S., 1991. Strain localization behaviour in experimental shear zones. Pure and Applied Geophysics 137, 421–438.

Jonas, J.J., 1993. Modelling the length changes that take place during torsion testing. International Journal of Mechanical Sciences 35, 1065–1077.

Keane, D.M., Sellars, C.M., Tegart, W.J. McG., 1966. High-temperature deformation of iron. In: Proceedings of the conference on 'Deformation under hot working conditions' held at the Department of Metallurgy, University of Sheffield, on 5 and 6 July 1966, pp. 21–28.

Kunze, K., Pieri, M., Burlini, L., Wenk, H.-R., 1998. EOS Transactions of the American Geophysical Union 79 (Fall Meeting Supplement), F851.

Lindholm, U.S., Nagy, A., Johnson, G.R., Hoegfeldt, J.M., 1981. Large strain, high strain rate testing of copper. Journal of Engineering Materials and Technology 102, 376–381.

Metals Handbook, 1985. Vol. 8. Mechanical Testing. American Society for Metals.

Montheillet, F., Cohen, M., Jonas, J.J., 1984. Axial stresses and texture development during the torsion testing of Al, Cu and Fe. Acta Metallurgica 32, 2077–2089.

Odqvist, F.K.G., 1935. Creep stresses in a rotating disc. In: Proceedings of the 4th International Congress on Applied Mechanics. Cambridge University Press, Cambridge, pp. 228–229.

Odqvist, F.K.G., 1966. Mathematical theory of creep and creep rupture. Oxford University Press, London.

Paterson, M.S., 1990. Rock deformation experimentation. In: Duba, A.G., Durham, W.B., Handin, J.W., Wang, H.F. (Eds.), The Brittle–Ductile Transition in Rocks. The Heard Volume, American Geophysical Union Geophysical Monograph, 56. AGU, Washington, DC, pp. 187–194.

Pieri, M., Stretton, I., Kunze, K., Burlini, L., Olgaard, D. L., Burg, J.-P., Wenk, H.-R., 2000. Texture development in calcite through deformation and dynamic recrystallization at 1000K during torsion to large strain. Tectonophysics (in press).

Ramsay, J.G., 1980. Shear zone geometry: a review. Journal of Structural Geology 2, 83–99.

Ramsay, J.G., Graham, R.H., 1970. Strain variation in shear belts. Canadian Journal of Earth Sciences 7, 786–813.

Ramsay, J.G., Huber, M.I., 1983. The Techniques of Modern Structural Geology. Volume 1: Strain Analysis. Academic Press, London.

Riecker, R.E., 1965. Fault plane features: an alternative explanation. Journal of Sedimentary Petrology 35, 746–748.

Riecker, R.E., Rooney, T.P., 1966. Weakening of dunite by serpentine dehydration. Science 152, 196–198.

Riecker, R.E., Rooney, T.P., 1967. Shear strength and weakening of zeolitized tuffs from the Nevada test site, Nevada. American Mineralogist 52, 1174–1178.

Riecker, R.E., Rooney, T.P., 1969. Water-induced weakening of hornblende and amphibolite. Nature (London) 224, 1299 (letter).

Riecker, R.E., Seifert, K.E., 1964a. Olivine shear strength at high pressure and room temperature. Geological Society of America Bulletin 75, 571–574.

Riecker, R.E., Seifert, K.E., 1964b. Shear deformation of upper-mantle mineral analogs: tests to 50 kilobars at 27°C. Journal of Geophysical Research 69, 3901–3911.

Rutter, E.H., 1974. The influence of temperature, strain rate and interstitial water in the experimental deformation of calcite rocks. Tectonophysics 22, 311–334.

Rutter, E.H., 1995. Experimental study of the influence of stress, temperature, and strain on the dynamic recrystallization of Carrara marble. Journal of Geophysical Research 100, 24651–24663.

Rutter, E.H., 1998. Use of extension testing to investigate the influence of finite strain on the rheological behaviour of marble. Journal of Structural Geology 20, 243–254.

Schmid, S.M., 1975. The Glarus overthrust: field evidence and mechanical model. Eclogae geologicae Helvetiae 68, 247–280.

Schmid, S.M., Boland, J.N., Paterson, M.S., 1977. Superplastic flow in fine grained limestone. Tectonophysics 43, 257–291.

Schmid, S.M., Panozzo, R., Bauer, S., 1987. Simple shear experiments on calcite rocks: rheology and microfabric. Journal of Structural Geology 9, 747–778.

Schmid, S.M., Paterson, M.S., Boland, J.N., 1980. High-temperature flow and dynamic recrystallization in Carrara marble. Tectonophysics 65, 245–280.

Stretton, I., Olgaard, D.L., 1997. A transition in deformation mechanism through dynamic recrystallization—evidence from high strain, high temperature torsion experiments. EOS Transactions of the American Geophysical Union 78 (Fall Meeting Supplement), F723.

Swift, H.W., 1947. Length changes in metals under torsional overstrain. Engineering (London) 163 (April 4), 253–257.

Tóth, L.S., Jonas, J.J., Daniel, D., Bailey, J.A., 1992. Texture development and length changes in copper bars subjected to free end torsion. Textures and Microstructures 19, 245–262.

Tullis, J., Yund, R.A., 1977. Experimental deformation of dry Westerly granite. Journal of Geophysical Research 82, 5705–5718.

Tullis, T.E., Weeks, J.D., 1986. Constitutive behavior and stability of frictional sliding of granite. Pure and Applied Geophysics 124, 383–414.

Tullis, T.E., 1994. The effect of pore fluid chemistry on the friction of quartz gouge. In: Hickman, S., Sibson, R., Bruhn, R. (Eds.), USGS Workshop LXIII: The mechanical involvement of fluids in faulting, June 1993, U.S. Geological Survey Open-file report, 94-228, pp. 509–513.

Van Arsdale, W.E., Hart, E.W., Jenkins, J.T., 1980. Elongation upon torsion in a theory for the inelastic behavior of metals. Journal of Applied Physics 51, 953–958.

Wendt, A.S., Olgaard, D.L., Mainprice, D., 1999. A technique for the fabrication of fully dense Ca-rich plagioclase (An^{70}–An^{100}) samples suitable for studying the plastic rheology of bytownite (An^{80}). Journal of Materials Science 34, 5733–5742.

Yund, R.A., Blanpied, M.L., Tullis, T.E., Weeks, J.D., 1990. Amorphous material in high strain experimental fault gouges. Journal of Geophysical Research 95, 15589–15602.

Zhang, S., Karato, S.-i., 1995. Lattice preferred orientation of olivine aggregates deformed in simple shear. Nature (London) 375, 774–777.